ISIJ International, Vol. 41 (2001), No. 10, pp. 1181–1193

Review

Mathematical Modeling of Fluid Flow in Continuous Casting

Brian G. THOMAS and Lifeng ZHANG

Department of Mechanical & Industrial Engineering, University of Illinois at Urbana-Champaign, 1206 West Green Street, Urbana, IL 61801 USA. E-mail: bgthomas@uiuc.edu

(*Received on April 5, 2001; accepted in final form on July 4, 2001*)

Fluid flow is very important to quality in the continuous casting of steel. With the high cost of empirical investigation and the increasing power of computer hardware and software, mathematical modeling is becoming an important tool to understand fluid flow phenomena. This paper reviews recent developments in modeling phenomena related to fluid flow in the continuous casting mold region, and the resulting implications for improving the process. These phenomena include turbulent flow in the nozzle and mold, the transport of bubbles and inclusion particles, multi-phase flow phenomena, the effect of electromagnetic forces, heat transfer, interfacial phenomena and interactions between the steel surface and the slag layers, the transport of solute elements and segregation. The work summarized in this paper can help to provide direction for further modeling investigation of the continuous casting mold, and to improve understanding of this important process.

KEY WORDS: mathematical modeling; computational simulation; review; continuous casting; nozzles; molds; multiphase; turbulent; fluid flow; electromagnetic; coupled solidification; inclusion entrapment; segregation.

1. Introduction

Fluid flow in continuous casting of steel is of great interest because it influences many important phenomena, which have far-reaching consequences on strand quality. They include:

- turbulent, transient fluid flow through a complex-geometry inlet nozzle into the mold cavity,
- the influence of operating parameters on these phenomena, including nozzle geometry, argon gas injection, and electromagnetic forces,
- the transport of argon bubbles through the turbulent liquid, their interaction with the flow and their possible entrapment in the solidifying shell,
- the transport of complex-shaped inclusion particles through the liquid, including the effects of buoyancy, turbulent interactions, and possible entrapment of the inclusions on nozzle walls, gas bubbles, solidifying steel interface, and the top surface,
- top surface contour and the behavior of the liquid slag layer, as related to flow and entrainment of the mold slag,
- transient fluctuations and waves in the top surface level, and their effect on surface defects,
- phenomena related to superheat transport including thermal buoyancy effects on the flow, meniscus freezing, shell thinning from the jet impinging upon the solidifying shell, and coupling with thermal stress analysis for crack prediction,
- nucleation, transport, and interaction of solid crystals, both in the flowing melt and against mold walls for microstructure prediction,
- solute transport, such as intermixing during a grade change and segregation.

Extensive past work has employed physical water models to successfully investigate fluid flow phenomena in the mold region of the continuous casting process.[1–16] The first study was carried out by Afanaseva *et al.*[1] for a straight bore nozzle system. Heaslip *et al.* extensively studied fluid flow in submerged entry nozzles under stopper-rod control and slide-gate control.[5,6] Gupta investigated the residence time distribution,[7] asymmetry and oscillation of the fluid flow pattern,[8,9] and slag entrapment.[10,11] Tanaka *et al*,[12] Teshima *et al*.[13] and Iguchi *et al.*[14] also used water models to study slag entrainment. Wang et al studied the influence of wettability on the behavior of argon bubbles and fluid flow.[15]

Although physical water models are well able to model single-phase fluid flow owing to the simulation kinematic viscosity of steel and water, the flow pattern itself is actually not of greatest interest. Furthermore, the physical bottom used in the water model interferes with the flow, the moving solidifying shell cannot be properly accounted, and properties related to other phenomena such as multiphase flow, heat transfer, and slag entrainment do not have proper similitude. Computational models based on finite-volume or finite-element solution of the Navier–Stokes equations can yield added insight into flow-related phenomena without these inaccuracies inherent in a water model.

In recent years, decreasing computational costs and increasing power of commercial modeling packages is making it easier to apply mathematical models as an additional tool to understand the process of the continuous casting of

steel. This paper will review recent developments in modeling each of the phenomena above, which are related to fluid flow in the continuous casting mold, and the resulting implications for improving the continuous casting process.

2. Fluid Flow Modeling

A typical three dimensional fluid flow model solves the continuity equation and Navier Stokes equations for incompressible Newtonian fluids, which are based on conserving mass (one equation) and momentum (three equations) at every point in a computational domain.[17,18] The solution of these equations, given elsewhere in this issue,[19] yields the pressure and velocity components at every point in the domain. At the high flow rates involved in this process, these models must incorporate turbulent fluid flow. Many different turbulence models have been employed by different researchers for fluid flow in continuous casting, such as effective viscosity models[20,21] (for the cylindrical mold and straight nozzle), one equation turbulence models (turbulent energy plus a given length-scale),[22] two-equation turbulence models such as the K–ε Model,[19,23] LES (Large Eddy Simulation),[24–28] possibly with a SGS (sub-grid scale) model,[29,30] and DNS (Direction Numerical Simulation).[19]

Among these models, direct numerical simulation is the simplest yet most computationally-demanding method. DNS uses a fine enough grid (mesh), to capture all of the turbulent eddies and their motion with time. To achieve more computationally-efficient results, turbulence is usually modeled on a courser grid using a time-averaged approximation, such as the popular K–ε model,[23] which averages out the effect of turbulence using an increased effective viscosity field, μ_{eff}. This approach requires solving two additional partial differential equations for the transport of turbulent kinetic energy and its dissipation rate.[19] The standard high-Reynolds-number K–ε model generally uses assumed "wall functions" to capture the steep gradients at wall boundaries, in order to achieve reasonable accuracy on a course grid.[23,31,32] Alternatively, the low-Reynolds-number turbulence model treats the boundary layer in a more general way, but requires a finer mesh at the walls. Large eddy simulation is an intermediate method between direct numerical simulation and K–ε turbulence models, which uses a turbulence model only at the sub-grid scale.[24–28]

Most previous flow models have used the finite difference method, owing to the availability of very fast and efficient solution methods.[33] Popular general-purpose codes of this type include CFX,[34] FLUENT,[35] FLOW3D,[36] and PHOENICS.[37] Special-purpose codes for mold filling in castings include MAGMASOFT[38] and PHYSICA,[39] which also solve for solidification, temperature evolution, and related phenomena. The finite element method, such as used in FIDAP,[40] can also be applied and has the advantage of being more easily adapted to arbitrary geometries, although

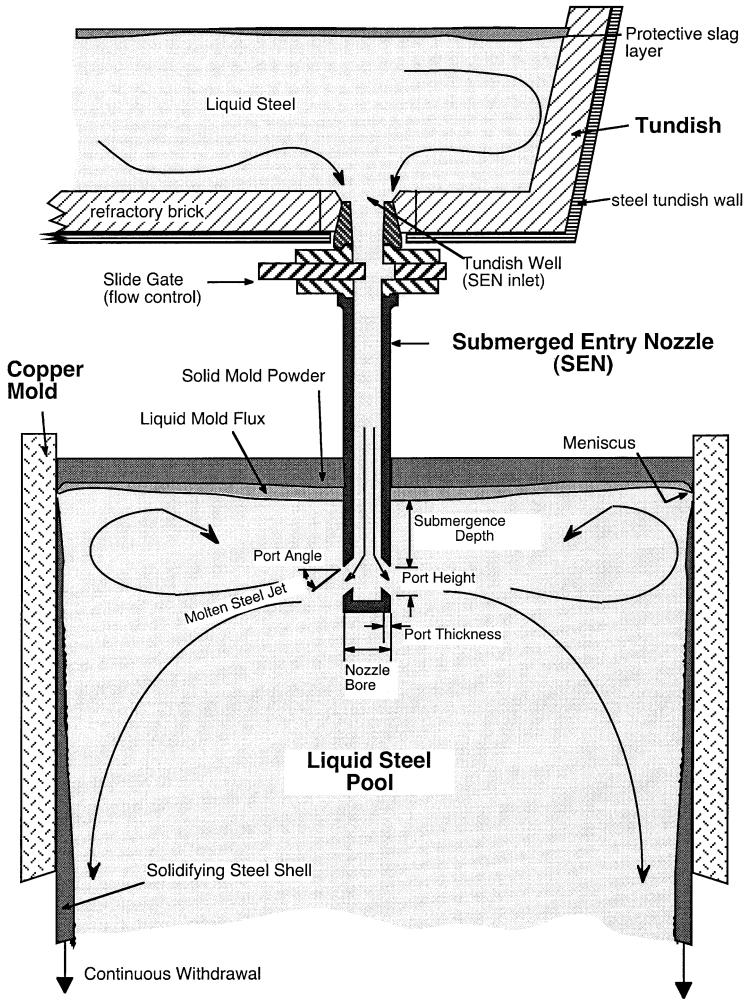

Fig. 1. Schematic of continuous casting process and terminology showing tundish, submerged entry nozzle, and mold.

it takes longer to execute. Special-purpose finite-element codes for casting include PROCAST[41] and CAFE.[42]

3. Fluid Flow in the Nozzle

The submerged entry nozzle (SEN) connects the tundish and mold, as shown in **Fig. 1**. Flow through the nozzle affects clogging, air aspiration, and most importantly, controls the flow conditions entering the mold. These conditions include the angle, speed, and biasing of the jets leaving each nozzle port, their level of turbulence, swirl and spread and the size and distribution of accompanying gas bubbles and inclusions. Accurate flow modeling requires careful attention to these inlet conditions, which is best achieved by extending the model upstream.

Significant work has been done in modeling flow through the nozzle.[22,30,32,43–51] As early as 1973, Szekely *et al*.[22] modeled the difference between fluid flow in the mold from a straight nozzle and that from a bifurcated nozzle. An extensive investigation of bifurcated nozzle flow was performed by Najjar *et al*.,[44] who explored the effects of nozzle shape, angle, height, width, ports thickness, bottom geometry, inlet velocity profile, and inlet shape. They concluded that the jet angle was controlled mainly by the port angle but was steeper with larger port area and thinner walls, and the degree of swirl was increased by larger or rounder ports. This work to characterize nozzle flow represents a critical first step towards a systematic modeling approach to SEN design.

Bai *et al*.[48–50] employed an Eulerian approach to investigate two-phase flow in the nozzle (**Fig. 2**[50]). They also validated the swirling velocity profile exiting the nozzle by comparing with measurements from Particle Image Velocity (PIV), which has been noted by others.[32,52] Most argon gas exits the upper portion of the nozzle port, while the main downward swirling flow contains very little. Gas injection bends the jet angle upward, enhances the turbulence level, and reduces the size of the back flow zone. They concluded that increasing argon injection might help to reduce air aspiration by increasing the minimum pressure below the slide gate. The results were further processed[50,51] using multivariable curve fitting methods to relate casting speed, argon injection rate, slide-gate opening position, nozzle bore diameter and tundish bath depth to air aspiration potential. The optimal argon flow rate depends on the casting speed, tundish level, and nozzle bore diameter.[50,51] Modeling based on high-speed video of water model experiments has revealed that the initial bubble size increases with increasing gas injection flow rate and decreasing liquid velocity, and is relatively independent of gas injection hole size and gas composition.[53,54]

4. Flow in the Mold

The first simulations of fluid flow and heat transfer in a cylindrical continuous casting mold with a straight nozzle, was carried out by Szekely and coworkers and assumed simple potential flow,[55] and later used one-equation turbulence models.[22,56] Yao *et al*.[29,30] published the first three-dimensional fluid flow simulation results for a rectangle mold and bifurcated nozzle system in 1984, which has since been

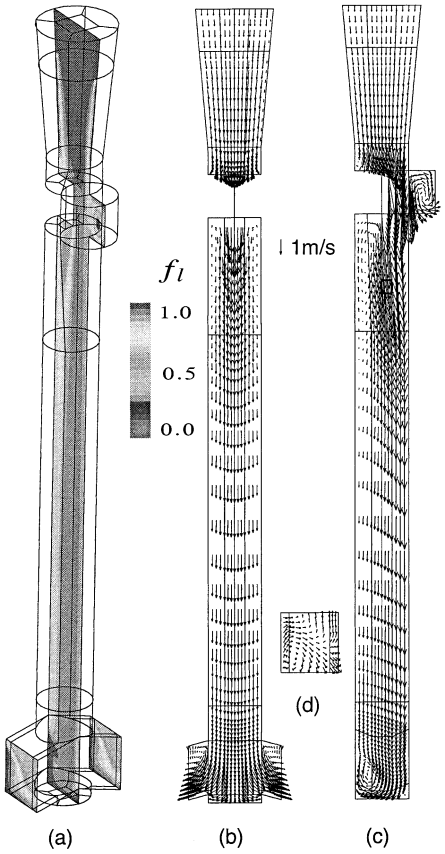

Fig. 2. Slide-gate nozzle calculations: (a) Argon gas distribution, (b) velocities in center plane parallel to WF, (c) velocities in center plane parallel to NF, (d) velocities at port outlet plane.[50]

modeled by many others, together with other phenomena as discussed later. Thomas and coworkers demonstrated the importance of the nozzle inlet conditions on mold flow, including K and ε inlet conditions.[45] Wall laws and the turbulent Prandtl number were also shown to be important.[31]

It is critically important to validate models with experimental measurement. Several methods have been employed to measure the fluid flow velocity vectors in continuous casting mold system, including LDV (Laser Doppler Velocimetry) for mold[16,57] and for SEN nozzle[58,59]), PIV (Particle Image Velocimetry),[19,25,60,61] hot wire anemometry[62]; and propeller flow meters.[63–65] **Figure 3** compares the instantaneous flow patterns predicted using physical and mathematical models for a typical double-roll flow pattern condition.[19] In this particular flow pattern, the steel jets first impinge on the narrow faces before turning upward towards the top surface and back across towards the SEN. Changing casting conditions (*e.g*. wider mold, shallower submergence, or adding gas) can reverse the flow pattern to single roll. In either case, the flow phenomena are more complex than indicated from the simple recirculation zones predicted by simple time-averaged flow models, with consequences for quality that demand further attention.

5. Transport of the Second Phase Particles (Bubbles and Inclusions)

Understanding the behavior of nonmetallic inclusions and bubbles, which accompany the flowing liquid in the

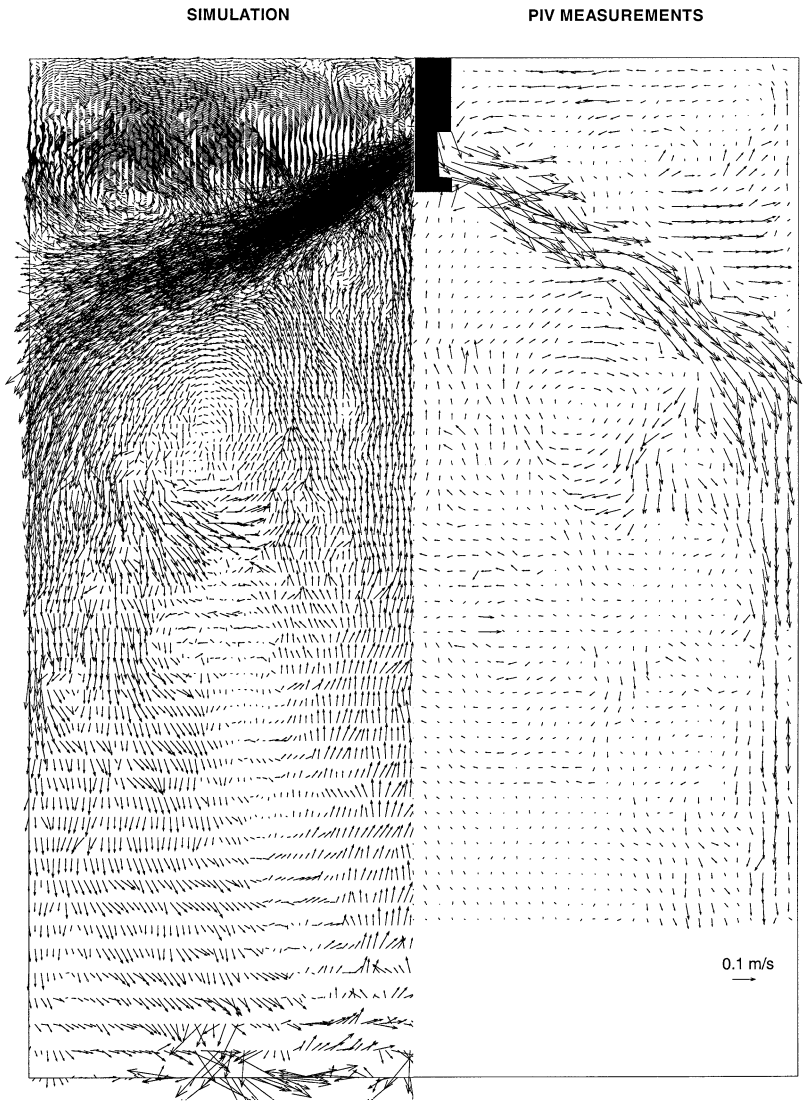

Fig. 3. Instantaneous flow pattern comparing LES simulation (left) and PIV measurement (right).[19]

continuous casting process, is important to cope with quality problems such as blisters in ultra-low carbon coils and inclusion defects in heavy plates. The jets of molten steel exiting the nozzle ports may carry argon bubbles and inclusions such as alumina into the mold cavity. Particles entrapped in the solidifying shell may create defects in the final product. Two main approaches have been applied to model the behavior of these second phase particles in continuous casting: the simple convective-diffusion approach and full trajectory calculations.

5.1. Convection-diffusion Approach

Particle (inclusion or bubble) motion in gas–liquid mixtures due to turbulent transport and diffusion can be modeled by solving a single transport equation for the continuum particle volume fraction,

$$\frac{\partial \sigma_P}{\partial t}+u_{iP}\frac{\partial \sigma_P}{\partial x_i}=\frac{\partial}{\partial_{x_i}}\left(D_{eff}\frac{\partial \sigma_P}{\partial x_i}\right) \quad \text{.....(1)}$$

where σ_P is the particle (inclusion or bubble) volume fraction; u_i is the known liquid velocity; D_{eff} is the effective diffusion coefficient; u_{iP} is the particle velocity, which equals the liquid velocity, except in the vertical direction, where the terminal rising velocity, V_T, should be added, namely, $u_{iP}=u_i+V_T$.

The first study of tracer dispersion and inclusion floatation in a continuous casting mold was made by Szekely *et al.*[55] When using this approach, the capture of inclusions to bubbles can be calculated simply by adding an additional source term to RHS of Eq. (1).[66,67] Particle entrapment by the solidifying shell can be modeled using a similar approach, by adding a negative source term to Eq. (1).[68] Several previous models assume that particles are entrapped every time they touch the solidification front.[66,67] However, particles which touch the solidifying front are not always engulfed unless their velocity is slow enough. The entrapment phenomenon is very complex and is receiving well-deserved attention in recent work.[69–71] This is needed for the development of improved entrapment criteria.

5.2. Trajectory Approach[49,56,62,72–74]

Particle trajectories can be calculated using the Langrangian particle tracking method, which solves a transport equation (Eq. (2)) for each particle as it travels through a previously calculated velocity field.

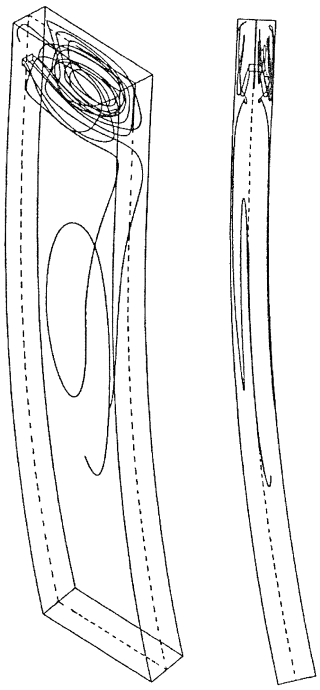

Fig. 4. Sample trajectories of five particles carried into the liquid pool.[49]

$$\frac{dv_{Pi}}{dt} = -\frac{3}{4}\frac{C_D v_{Pi}\rho}{d_P \rho_P}\left|v_{Pi} - u_i\right| + \frac{(\rho_P - \rho)g}{\rho_P} + C_A\left(\frac{du_i}{dt} - \frac{dv_{Pi}}{dt}\right) \quad \text{.....(2)}$$

where ρ_P and ρ are the particle and liquid densities, v_{Pi} is the particle velocity, C_D is the drag coefficient as a function of particle Reynolds number, C_A is a constant, g is gravity acceleration. The first term on the right of this equation is the drag force, which is always opposite to the motion direction. The second term is the buoyancy force due to gravity, and the third term is the "added mass force". The trajectory of each particle can then be calculated incrementally by integrating its local velocity.

The effects of turbulent motion can be modeled crudely from a K–ε flow field by adding a random velocity fluctuation at each step, whose magnitude varies with the local turbulent kinetic energy level.[49] To obtain significant statistics, the trajectories of several hundred individual particles should be calculated, using different starting points. An early inclusion trajectory calculation in the continuous casting mold was made by Asai *et al.*[56] **Figure 4** shows example trajectories of several inclusions moving through a steady flow field.[49]

Steeper nozzle port angle is reported to prolong the residence time of inclusions and thereby aid in their removal.[73] Higher casting speed shortens the residence time but is disadvantageous to inclusion removal.[73] A more desirable casting condition seems to deep nozzle submergence with an upward angle of nozzle port.[73] Large inclusions are likely to become entrapped just below the mold by following a spiral path while traveling with the liquid in the lower recirculating zone and simultaneously floating toward the inner radius shell of the wide face.[62] Mold curvature makes inclusion entrapment by the shell on the inner-radius of the wide face easier, consequently making floatation to the top slag layer less likely.[62] The calculations of Hwang's group[73,74] with this trajectory approach indicates that only 20% of 10 μm diameter inclusions are removed, while more than 70% of 50 μm inclusions are removed during continuous casting (160 mm diameter billet, straight nozzle with 150–180 mm submergence depth, and 1.5–1.8 m/min casting speed).[74]

An important modeling issue is the capture of inclusions by attachment to bubbles, which float more quickly and thereby increase inclusion removal rates. As an initial step for the trajectory approach, Thomas *et al.*[49] predict the attachment of inclusions to an argon gas bubble rising at constant velocity relative to the surrounding liquid steel, assuming that the bubble is a sphere submerged in inviscid (potential) flow of constant local velocity.

Most of the argon bubbles circulate in the upper mold area and float out to the top surface,[49] but a few might be trapped at the meniscus if there is a solidification hook, leading to surface defects. A few small bubbles manage to penetrate into the lower recirculation zone, where they move in a similar manner to large inclusion clusters.[49] Modeling and measurements together have revealed that these bubbles are trapped 2–3 m below the meniscus.[49]

All of the diffusion and trajectory models indicate that small inclusion particles are more likely to become entrapped within the mushy zone than large particles. Inclusions that rise through stagnant molten steel faster than the casting speed are reported to be almost completely removed by the installation of vertical mold walls.[75] The vertical section needed to promote the flotation and removal of inclusion is less than 2.5 to 3.0 m, irrespective of inclusion size and casting speed.[75]

6. Multiphase Fluid Flow Models

Several different methods have been developed to model multiphase flow in continuous casting in order to take into account the important effect of bubble movement on the liquid flow field.

6.1. Algebraic Slip Model (ASM)[53,62,64–66,76,77]

This method approximates the dispersed two-phase system as a single-phase mixture of liquid and gas. Flow of the liquid–gas mixture is calculated by solving only one continuity equation, one set of momentum equations, and one set of turbulence equations. The gas fraction is calculated from one additional transport equation for the gas phase: Eq. (1). The slip velocity of the argon bubbles depends on their size and shape. Usually, their terminal velocity is used.[68] The buoyancy effect of the gas bubbles on the fluid flow is taken into account by adding an extra force term to the vertical momentum equation: $S_{gz} = -\sigma_g g\rho$, where σ_g is the gas volume fraction.

An enhancement to this procedure is the Eulerian "homogeneous model" which still solves only a single set of transport equations, but adopts mixture properties where the density and viscosity are proportional to the volume fraction of the phases. The volume fractions vary within each cell, but always sum to one. Models of this type have

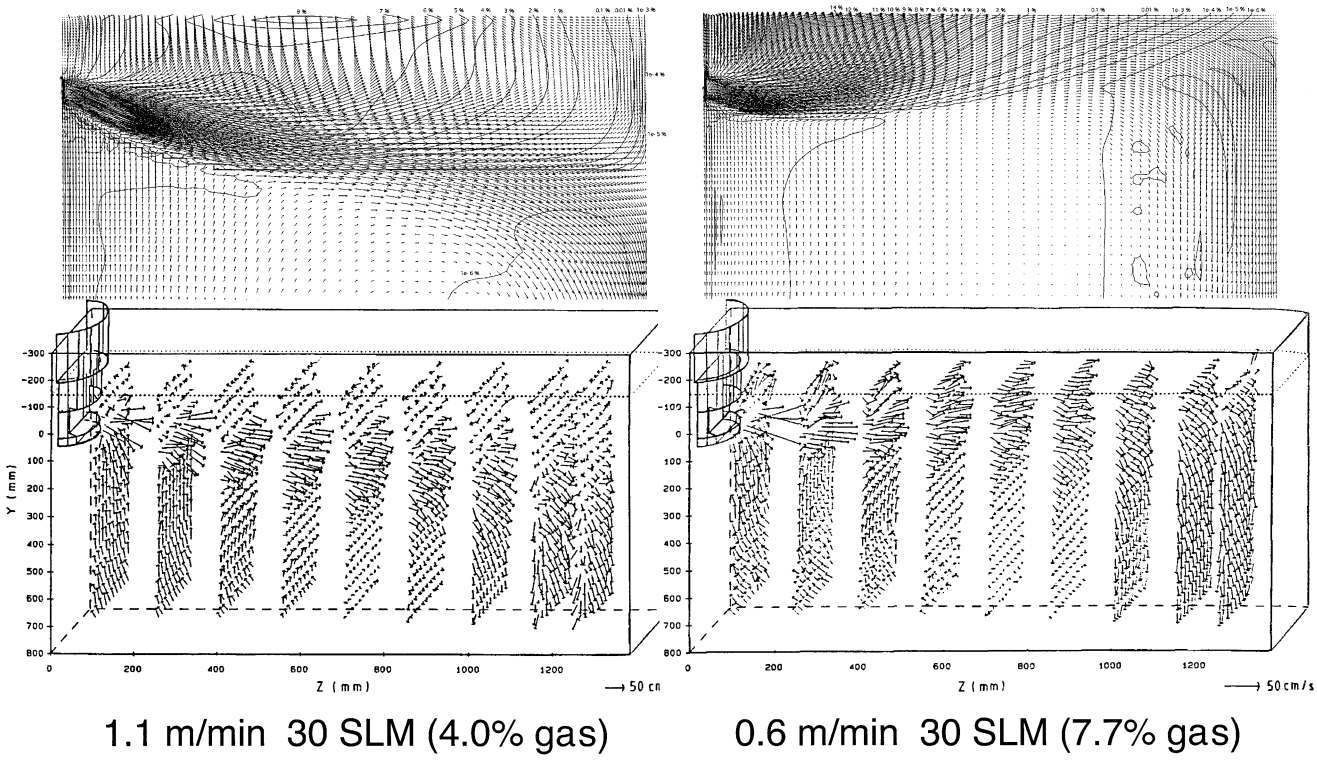

Fig. 5. The effect of argon on flow in the mold, comparing k–ε simulations (above)[88] and water model observations (below).[63]

been applied to model the effect of argon gas in continuous casting of steel slabs.[78,79]

6.2. Langrangian Two Phase Model

In this approach, only one velocity field of the liquid is solved, but the liquid volume fraction is included in every term. The liquid volume fraction is calculated from the gas volume fraction, which is solved using the particle trajectory Eq. (2). This model has been used to calculate two-phase fluid flow in a continuous casting mold.[80]

6.3. Eulerian Two-phase Model[49,81–83]

In this model, one velocity field for the liquid steel and another separate velocity field for the gas phase are solved. The momentum equation for each phase is affected by the other phase through inter-phase drag terms. Several studies of multiphase flow phenomena in continuous casting of steel have employed models of this type.[49–51,82,84,85] Bubble induced turbulence may be added to the K and ε equations through source terms.[86,87]

Argon bubbles alter the flow pattern in the upper recirculation zone, shifting the impingement point and recirculation zone upward. The lifting effect increases with increasing gas fraction, increasing mold width, decreasing casting speed and decreasing bubble size. The effect is substantial, as a slight increase in gas fraction is sometimes enough to completely reverse the flow pattern from double roll to single roll, as shown in **Fig. 5**.[88] An important issue is the particle size distribution. The bubble size greatly affects both the fluid flow pattern,[53] and inclusion removal by attachment to the bubbles.[89] Particle size distributions have been measured[54,90] and modeled,[54] but have been given relatively little attention in particle flow modeling studies to date.

7. Effect of Electromagnetic Forces

The application of magnetohydrodynamics (MHD) to control the flow of molten steel in the continuous casting process started with electromagnetic stirring (EMS) of the strand pool with a traveling (alternating) magnetic field. It has now advanced to electromagnetic stirring in the mold and to an in-mold direct-current magnetic field, which induces a braking force to slow the flow (EMBr). These technologies are reported to improve the surface quality of cast steel by homogenizing the meniscus temperature, stabilizing initial solidification, and cleaning the surface layer. They may also improve the internal quality of cast steel by preventing inclusions from penetrating too deep into the pool and promoting the flotation of argon bubbles.

Owing to the difficulty of conducting measurements, development of EMS and EMBr must rely heavily on computational modeling. The flow pattern and mixing under the application of electromagnetic forces can be modeled by solving the Maxwell, Ohm, and charge conservation equations for electromagnetic forces simultaneously with the flow model equations.[91]

As early as 1986, Spitzer *et al.*[92] calculated the three-dimensional flow field in rotational electromagnetic stirring of round steel strands and discussed the influence of stirrer position, stirring length, and electromagnetic parameters on the flow field. Since then, many other industrial studies have gained important insights from three dimensional coupled analysis of the mold flow pattern.[93,94]

Yao *et al.*[29] appear to have applied the first 3-D computation to study the effect of electromagnetic braking (EMBr) on fluid flow in the continuous casting mold region. Hwang *et al.*[77] modeled fluid flow, induced current, argon gas fraction in the molten steel, and meniscus shape together to

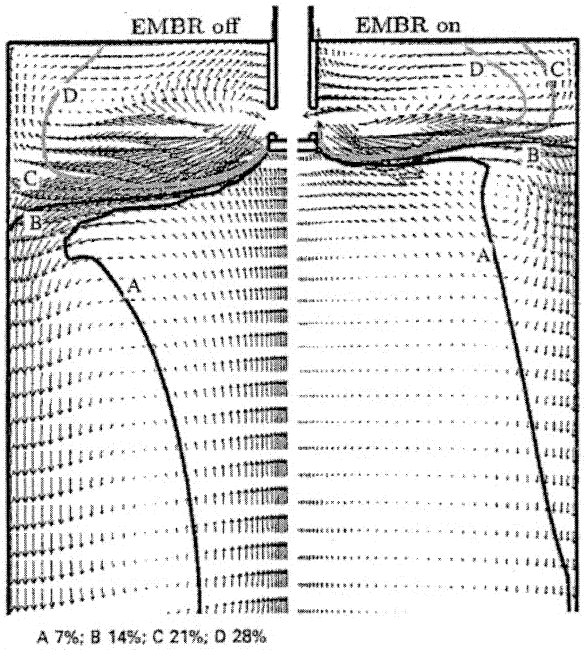

Fig. 6. The effect of EMBr on velocity and concentration profiles of 350 μm argon bubbles in 1 700 mm wide mold.[68]

study the effect of EMBr. Their investigation focussed attention on several evaluation standards: average velocity beneath the meniscus, the shape of the meniscus, and the standard deviation of velocities in the casting direction. Although gas buoyancy still has an important effect on the flow, it is reported[79] that magnetic-field application can significantly suppress its effect. The modeled effect of EMBr to decrease downward fluid flow velocities and reduce the depth of bubble penetration is shown in **Fig. 6**.[68] This may reduce inclusions and pinholes at the inside 1/4 accumulation zone of the curved-type slab conditions caster.

A novel application of electromagnetic forces is the development of simultaneous casting of plain steel with a stainless-steel surface layer, using two nozzles with different submergence.[95] To prevent mixing due to momentum and density-driven flow, development of this process is aided by modeling the fluid momentum equations coupled with both electromagnetic and heat transfer equations.[95]

8. Heat Transfer Related Phenomena

Fluid flow models can be extended to predict the dissipation of superheat, and/or temperature evolution in the solidifying steel shell by solving an additional equation for heat transport,

$$\frac{\partial}{\partial t}(\rho H)+\frac{\partial}{\partial x_i}(\rho u_i H)=\frac{\partial}{\partial x_i}(k_{\text{eff}})\frac{\partial T}{\partial x_i}+Q \quad \text{.....(3)}$$

where H is enthalpy or heat content (J/kg), u_i is velocity in x_i direction (m/s), k_{eff}, is temperature-dependent effective thermal conductivity (W/m·K), T is the temperature field (K), and Q contains heat sources (W/m^3).

The first study model of fluid flow coupled with heat transfer and solidification in the continuous casting mold was by Szekely and coworkers, first assuming potential flow,[55] and later using a full turbulence model.[4,56]

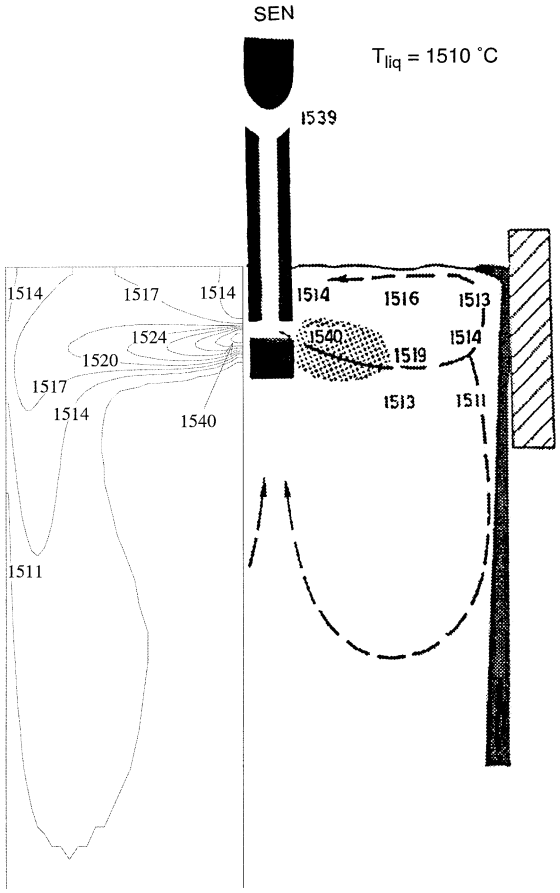

Fig. 7. Temperature distribution in mold showing superheat dissipation.[103]

Choudhary *et al.*[20,21] modeled turbulent flow and energy transport within the mushy region using a fully-coupled model and compared with experimental data.

8.1. Superheat Transfer and Solidification

An important task of the flow pattern is to deliver molten steel to the meniscus region that has enough superheat during the critical first stages of solidification. Superheat is the sensible heat contained in the liquid metal above the liquidus temperature and is dissipated mainly in the mold. The transport and removal of superheat is modeled by solving Eq. (3) using the velocities found from the flow model. The effective thermal conductivity of the liquid is proportional to the effective viscosity, which can be found from the turbulence parameters (K and ε). In order to account for the effect of the solid matrix on fluid flow in the mushy region, the enthalpy-porosity technique has been employed, wherein a source term, derived from Darcy's law of porous media, is incorporated in the momentum equation.[72,96] Many researchers model flow and solidification as a coupled problem on a fixed grid.[97–99] Although very flexible, this approach is subject to convergence difficulties and requires a fine grid to resolve the thin porous mushy zone next to the thin shell.

An alternative approach for columnar solidification of a thin shell, such as found in the mold for the continuous casting of steel, is to treat the boundary as a rough wall fixed at the liquidus temperature using thermal wall laws.[100–102] **Figure 7** compares calculations using this ap-

proach with measured temperatures in the liquid pool.[103] The coldest regions are found at the meniscus at the top corners near the narrow face and near the SEN. This is a concern because it could lead to freezing of the meniscus or a thick flux rim, leading to quality problems such as deep oscillation marks, cracks and other surface defects.

Figure 7 also shows that the temperature drops almost to the liquidus by mold exit, indicating that most of the superheat is dissipated in the mold. The results of Thomas and coworkers[100–102] indicate that the maximum heat input to the shell occurs near the impingement point on the narrow face and confirm that most of the superheat is dissipated in or just below the mold. Superheat temperature and casting speed have the most important and direct influence on heat flux.[102] This effect is important because delivering superheat to the inside of the shell can retard solidification significantly, which has been demonstrated through comparison with measurements of heat flux and breakout shells.[100,101,104]

8.2. Thermal Buoyancy Effect

The influence of thermal buoyancy is of critical importance to flow in ladles and tundishes. It is less important in the mold and upper strand, where the fluid momentum controls the flow pattern. Nevertheless, Khodadadi *et al.*[105] modeled the effect of thermal buoyancy on fluid flow in a continuous casting mold by adding a buoyancy source term to the vertical momentum equation and also modifying the K and ε equations. Aboutalebi *et al.*,[72,96] modeled flow coupled with both thermocapillary and buoyancy effects to study the influence of liquid surface tension gradients across the meniscus surface, and natural convection on flow patterns in the liquid pool. Turbulence reduces temperature gradients in the liquid pool, but is unable to penetrate the mushy zone, where high gradients exist. The effect of the natural convection may be appreciable in the submold region, where forced convection is small and flow is driven mainly by thermal and solutal buoyancy. This phenomenon is likely very important in determining flow for macrosegregation studies.

8.3. Coupled Thermal-mechanical Behavior of the Shell

The solidifying shell is prone to a variety of distortion, cracking, and segregation problems, which are influenced in part by fluid flow phenomena. To investigate these problems, models are being developed to simulate fluid flow coupled together with thermal and mechanical behavior of the solidifying steel shell during continuous casting of both billets[106–108] and slabs.[109–114] Transient temperature, flow and pressure calculations have also been applied in the slag layers, to study complex phenomena such as oscillation mark formation at the meniscus.[115]

Figure 8 presents a sample horizontal section of temperature and distorted shape of the solidifying shell, calculated with a coupled thermal-stress model which incorporated the effects of the turbulent flow.[109] To achieve reasonable accuracy, a very fine mesh and small time steps are needed. Of greatest interest is the thin region on the off-corner narrow face, where the superheat delivered from the impinging steel jet is much greater than the heat extracted by the mold across the air gap. The result was a breakout at that location.

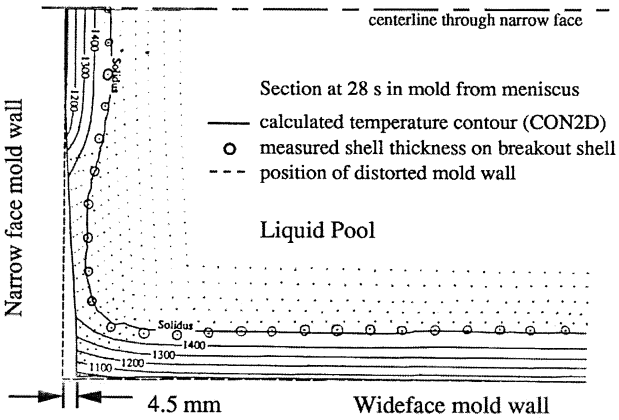

Fig. 8. Comparison of predicted and measured shell growth in a horizontal section through the center of continuous-casting steel breakout shell.[109]

Lee *et al.*[107] developed a model to predict the possibility of cracks in the strand, originated from the interdendritic liquid film in the mushy zone, through the fully coupled analysis of fluid flow, heat transfer and stress in the continuous casting billet. One crack susceptibility coefficient, which is the ratio between the analyzed maximum principal stress and the critical yield strength for the cracking, is employed. Results indicate that the surface crack could form at the initial stage of casting and the internal crack could be found at the middle stage of casting.

Computational models also can be applied to calculate thermomechanical behavior of the solidifying shell below the mold. Models can investigate shell bulging between the support rolls due to ferrostatic-pressure induced creep,[116–120] and the stresses induced during unbending.[121] These models are important for the design of spray systems and rolls in order to avoid internal hot tear cracks and centerline segregation. These models face great numerical challenges because the phenomena are generally three dimensional and transient, the constitutive equations are highly nonlinear, and the mechanical behavior in one region (*e.g.* the mold) may be coupled with the behavior very far away (*e.g.* unbending rolls).

9. Phenomena of Free Surface, Slag Layer, and Interface

Understanding of steel-slag interface surface wave behavior and the mechanisms that remove particles or breakup the interface leading to slag entrainment, is very important to steel continuous casting quality. There are several approaches to predicting the interface wave height and level fluctuations.

9.1. Analytical Solutions

The results of a flow simulation may be assessed quickly using crude analytical calculations based on surface pressure differences and stability criteria. Huang *et al.*[78] matched such interface shape predictions with experimental measurements of level fluctuations in a water model by Teshima.[13] The latter developed correlations to predict fluctuations as a function of casting conditions which was validated with plant experiments. These methods are also

crucial for investigating complex phenomena, such as oscillation marks.[115]

Rottman[122] developed an analytical solution for the maximum standing wave height prior to the onset of wave instability and breakup. Using a water/oil model, Gupta *et al.*[11, 123] measured the ratio of interface wave amplitude to nozzle exit diameter to be about $0.6Fr_m$, where $Fr_m=(V^2_{port}/gL_c)\cdot(\rho/\Delta\rho)$ and V_{port} is port exit velocity, $\Delta\rho$ is the density difference between the slag and liquid phases, and L_c is the height of the upper recirculation zone. Bergeles and coworkers applied these two findings together with interface simulation results to predict that wave instability and emulsification will occur when Fr_m exceeds 4.523 for a typical 3-D steel–slag system.[124]

9.2. VOF (Volume Of Fluid) Method[125]

This popular method, originally developed by Hirt *et al.*[125] tracks a free surface moving through the computational grid by simultaneously solving for another parameter, the volume of fluid per unit volume, f_i. This requires satisfaction of an additional conservation equation, such as:

$$\frac{\partial f_i}{\partial t}+\left[\frac{\partial}{\partial x_i}(f_i u_i)\right]=0 \quad \text{.....(4)}$$

This appears to be the first method applied to numerically simulate the important shape of the free surface in the continuous casting mold.[73,74,84] Ilegbusi *et al.*[84] found that the velocity field in an electromagnetically-stirred cylinder, was markedly different when the free surface contour was calculated, than for a flat surface. The VOF method also has been applied to gas bubble formation in the nozzle.[54]

9.3. SLIC (Simplified Line-interface Calculation) Method[126]

In this variation of the VOF method, the steel/slag interface is tracked using the volume fraction of the liquid phase, *C*. A single set of flow equations are solved, but the density is adjusted using a weighted average, $\rho=\rho_l C+\rho_s(1-C)$. The SLIC method is a direction-spilt algorithm, and the interface surface (or the free surface) in a grid cell is approximately constructed by straight lines parallel to one coordinate direction, using the volume fractions of the central and two adjacent cells in each direction. Therefore, an interface call may have a different representation for each direction sweep. The flux of either fluid through the interface cell faces is then calculated from the displacement of a rectangular fluid box that moves with the mean flow velocities (resulting from the solution of the transport equations). A typical simulation result including the interface shape is shown in **Fig 9**.[126] The amplitude of the interface wave increases as the immersion depth of the SEN decreases. The wave height increases also with the casting speed, but with a rate smaller than the square of the bulk inlet velocity in the SEN.[126]

9.4. ALE (Arbitrary Lagrangian–Eulerian) Method[127]

This method, originally developed by Hirt *et al.*,[127] employs a structured computational grid which deforms during the solution procedure or with time in order to adjust the local shape of the free surface or interface to maintain a constant interface pressure. This approach benefits from maintaining a sharp interface, relative to the VOF method. When both liquid steel and slag are modeled, they cannot intermix, and a second top free surface may be employed. This method has been applied to continuous casting in several flow model studies.[83,124,128] Bergeles *et al.*[124,129] quantified the great variations in interfacial steel–slag wave shape, while finding the slag surface to remain almost undisturbed.

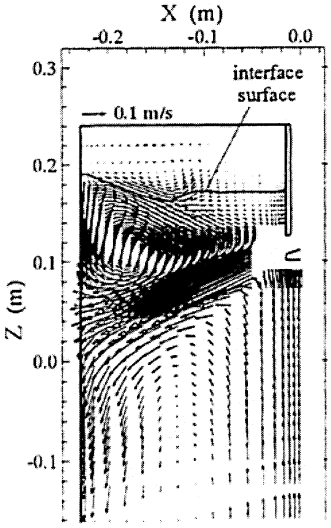

Fig. 9. Predicted flow field and interface shape (24 *l*/min and 50 mm submergence depth).[126]

9.5. Pressure Balance Method[77]

A cruder version of the ALE method has been used to predict the top interface shape in the continuous casting mold.[66,77] Starting with a calculation of the flow field and argon gas distribution, the hydrostatic pressure P_g on the surface of molten steel is then calculated. The dynamic pressure P_d is given from the previous flow calculation, ignoring the small effect of surface tension. Next, the displacement of every meniscus node is determined by satisfying the requirement that $P_g+P_d=$constant. Finally, a new grid is constructed based on this displacement and iteration is repeated until the displacement change is less than a convergence criterion.

The flow of steel in the upper mold may influence the top surface powder layers, which are very important to steel quality. Mold powder is added periodically to the top surface of the steel. It sinters and melts to form a protective liquid flux layer, which helps to trap impurities and inclusions. This liquid is drawn into the gap between the shell and mold during oscillation, where it acts as a lubricant and helps to make heat transfer more uniform. When a slag layer is present, the pressures on each of the steel/slag interface are made to balance. One such study with this method assumed a planer top surface of the slag layer.[66]

The results in **Fig. 10**[130,131] show that for typical double-roll flow, the momentum of the flow up the narrow face raises the level of the interface there. The model used in this calculation features different temperature-dependent flux properties for the interior, where the flux viscosity during sintering before melting, compared with the region near the narrow face mold walls, where the flux resolidifies to form a solid rim. The shear stress along the interface is de-

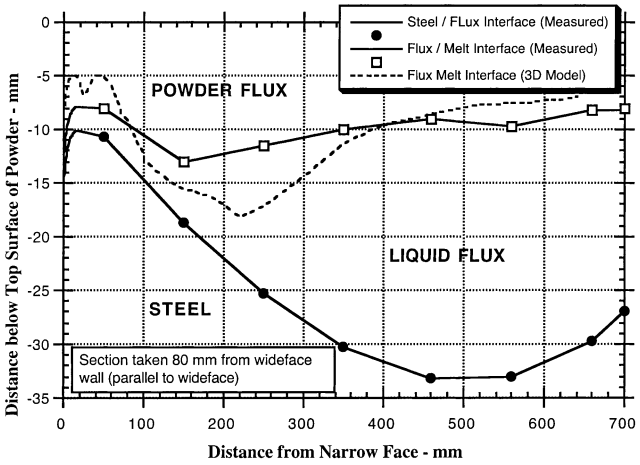

Fig. 10. Comparison of measured and predicted melt-interface positions[130)]

termined through coupled calculations with a 3-D steady flow model. The shear forces, imposed by the steel surface motion towards the SEN, create a large recirculation zone in the liquid flux pool. Its depth increases with increasing casting speed, increasing liquid flux conductivity, and decreasing flux viscosity.

Interface shape is important because it affects surface defects, through level fluctuations, and mold–slag entrapment. Slag entrapment leads to serious internal defects in steel sheet product and is caused by excessive flow across the meniscus, argon bubble bursting at the meniscus, or by vortexes near the immersion nozzle associated with asymmetric flow. Tanaka *et al.*[12)] found from water model experiments that vortex depth increases in proportion to the square of the exit port velocity, decreases with deeper nozzle immersion and also depends on the slag viscosity. Phenomena such as these are difficult to measure or to accurately quantify with a physical model, so are worthy of mathematical modeling. For example, a model of inclusion entrainment from the slag layer was developed by Bouris *et al.*[132)]

10. Solute Transport Phenomena

The equation for turbulent transport and diffusion of solute elements in liquid steel of a continuous casting mold and slab is the same as Eq. (1) except that concentration is the unknown field variable and u_{ip} is always equal to u_i. Composition variation during grade changes and segregation are two important applications of solute transport models, which require a previous simulation of flow field.

Large composition differences can arise through the thickness and along the length of the final product due to intermixing after a change in steel grade during continuous casting. Models to predict intermixing must first simulate composition change in both the tundish and in the liquid core of the strand as a function of time. In order to predict the final composition distribution within the final product, a further model must account for the cessation of intermixing after the shell has solidified.[133–136)]

Figure 11 shows example composition distributions in a continuous cast slab calculated using such a model.[133,134)] To ensure accuracy, extensive verification and calibration

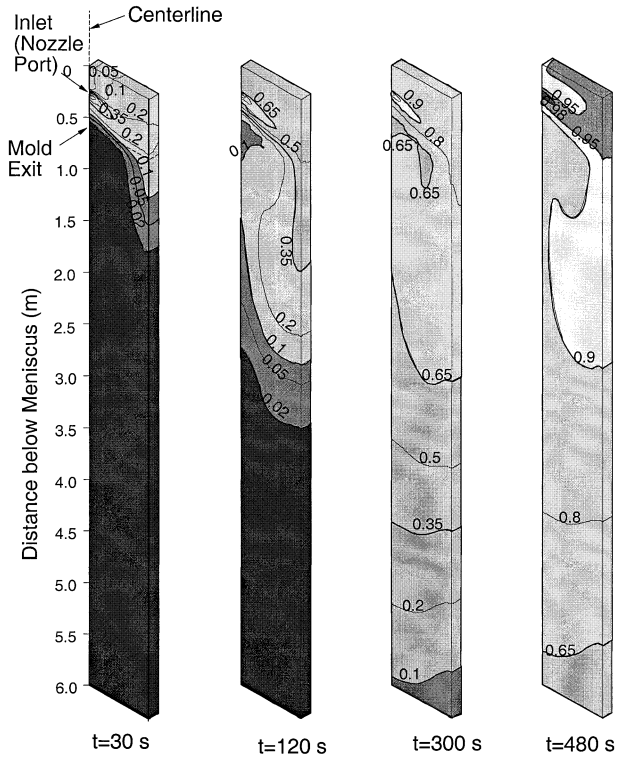

Fig. 11. Relative concentration of new steel in strand during grade change[133)]

were undertaken for each submodel.[134)] The results in Fig. 11 clearly show the important difference between centerline and surface composition. New grade penetrates deeply into the liquid cavity and contaminates the old grade along the centerline. Old grade lingers in the tundish and mold cavity to contaminate the surface composition of the new grade. This difference is particularly evident in small tundish, thick-mold operations, where mixing in the strand is dominant.[135)] Higher casting speed increases the extent of intermixing. Mold width, ramping of casting speed, and nozzle design have only small effects. Slab thickness, however, significantly influences the intermixing length of the slab. The axial transport of solute due to turbulent eddy motion was found to be many orders of magnitude greater than molecular diffusion and thus dominates the resulting composition distribution.[133)]

Macrosegregation is detrimental to product properties, particularly for highly alloyed steels which experience the most segregation. Cracks which fill with enriched interdendritic liquid present a macrosegregation problem that is worse than simple cracking. Segregation near the centerline of the solidified slab can be reduced through careful application of eletromagnetic forces, and soft reduction, where the slab is rolled or quenched just before it is fully solidified. Modeling is needed to help understand and optimize these processes.

Macrosegregation is very difficult to simulate, because such a wide range of coupled phenomena must be properly modeled. Firstly, solute transport occurs on vastly different length scales, starting with microsegregation. The fundamental cause of macrosegregation is fluid flow driven by convection, bulging between rolls, solidification shrinkage, and thermal stress. Increasing superheat tends to worsen

segregation, so even the details of mold superheat transfer are important. These phenomena must all be modeled accurately.

The microstructure is also important, because equiaxed crystals behave differently than columnar grains, which must also be modeled. During the initial fraction of a second of solidification at the meniscus, a slight undercooling of the liquid is required before nucleation of solid crystals can start. The nuclei rapidly grow into dendrites, which evolve into grains and microstructures. These small-scale phenomena can be modeled using microstructure models such as the cellular automata[97] and phase field1[37] methods. The latter requires coupling with the concentration field on a very small scale so is very computationally intensive. Microstructure modeling is also greatly complicated by the macroscopic flow phenomena, including the convection of crystals in the molten pool in the strand, which depends on both flow from the nozzle and thermal/solutal convection.

Computational modeling of centerline macrosegregation in steel was pioneered by Miyazawa and Schwerdtfeger.[138] Recent models have taken additional steps to model this daunting problem.[99,139–141] Further explanation can be found in recent reviews of macrosegregation, by Flemings,[142] and its modeling, by Beckermann.[143]

Much further work is needed to understand and qualify these phenomena and to apply the results to optimize the continuous casting process. In striving towards these goals, the importance of combining modeling and experiments together cannot be overemphasized.

11. Conclusion

This article has shown the significant progress that has been achieved in the mathematical modeling of the continuous casting process. As increasing computational power and simulation tools continue to advance, modeling should play an increasing role in augmenting traditional research methods to achieve future advances to this important technology. Advanced computational flow modeling areas that should make increasing contributions include transient flow simulation, mold flux behavior, increased coupling with other phenomena, online quality prediction and control, especially for new processes such as high speed billet casting, thin slab casting, and strip casting.

Despite these advances, much further work is needed before models will reach their full potential. For example, future multiphase flow models should consider particle size distributions, which evolve according to collision and agglomeration phenomena. Particle entrapment phenomena, including emulsification of the slag and interface need much more development, based on experiments. More validation with both laboratory and plant experiments are needed to make models fully quantitative. Many more parametric studies with advanced models are needed to find optimal conditions. The final test of a model is if the results can be implemented into practice and improvements can be achieved, such as the avoidance of defects in the steel product. Plant trials are ultimately needed for this implementation. Successful trials will come from people with good ideas based on insights supplied from all available sources, including previous literature, experience, physical models, and mathematical models.

Acknowledgements

The authors wish to thank the National Science Foundation (NSF-Grant # DMI—98-00274) and the Continuous Casting Consortium at the University of Illinois at Urbana-Champaign for support of this work.

REFERENCES

1) K. I. Afanaseva and T. P. Iventsov: *Stal*, **18** (1958), No. 7, 599.
2) N. T. Mills and L. F. Barnhardt: *J. Met.*, **23** (1971), No 11, 37.
3) N. T. Mills and L. F. Barnhardt: Open Hearth Proceedings, Vol. 54, TMS-AIME, Warrendale, PA, (1971), 303.
4) J. Szekely and R. T. Yadoya: *Metall. Trans. B*, **3** (1972), No. 5, 2673.
5) L. J. Heaslip and J. Schade: *Iron Steelmaker* (*ISS Transactions*), **26** (1999), No. 1, 33.
6) L. J. Heaslip, I. D. Sommerville, A. McLean, L. Swartz and W. G. Wilson: *Iron Steelmaker* (*ISS Transactions*), **14** (1987), No. 8, 49.
7) D. Gupta, S. Subramaniam and A. K. Lahiri: *Steel Res*., **62** (1991), No. 11, 496.
8) D. Gupta, S. Chakraborty and A. K. Lahiri: *ISIJ Int*., **37** (1997), No. 7, 654.
9) D. Gupta and A. K. Lahiri: *Metall. Mater. Trans. B*, **27B** (1996), No. 5, 757.
10) D. Gupta and A. K. Lahiri: *Metall. Mater. Trans. B*, **27B** (1994), No. 4, 695.
11) D. Gupta and A. K. Lahiri: *Ironmaking Steelmaking*, **23** (1996), No. 4, 361.
12) H. Tanaka, H. Kuwatori and R. Nisihara: *Tetsu-to-Hagané*, **78** (1992), No. 5, 761.
13) T. Teshima, J. Kubota, M. Suzuki, K. Ozawa, T. Masaoka and S. Miyahara: *Tetsu-to-Hagané*, **79** (1993), No. 5, 576.
14) M. Iguchi, J. Yoshida, T. Shimzu and Y. Mizuno: *ISIJ Int*., **40** (2000), No. 7, 685.
15) Z. Wang, K. Mukai and D. Izu: *ISIJ Int*., **39** (1999), No. 2, 154.
16) M. Iguchi and N. Kasai: *Metall. Mater. Trans. B*, **31B** (2000), No. 3, 453.
17) S. V. Patankar and B. D. Spalding: *Int. J. Heat Mass Transfer*, **15** (1972), No. 10, 1787.
18) S. V. Patankar: Numerical Heat Transfer and Fluid Flow, McGraw Hill, New York, NY, (1980).
19) B. G. Thomas, Q. Yuan, S. Sivaramakrishnan, T. Shi, S. P. Vanka and M. B. Assar: *ISIJ Int*., **41** (2001), No. 10, 1262.
20) S. K. Choudhary and D. Mazumdar: *ISIJ Int*., **34** (1994), No. 7, 584.
21) S. K. Choudhary and D. Mazumdar: *Steel Res*., **66** (1995), No. 5, 199.
22) J. Szekely and R. T. Yadoya: *Metall. Mater. Trans*., **4** (1973), No. 5, 1379.
23) B. E. Launder and D. B. Spalding: *Comp. Meth. Appl. Mech. Eng*, **13** (1974), No 3, 269.
24) J. Smagorinsky: *Monthly Weather Review*, **91**, (1963), 99.
25) S. Sivaramakrishnan, B. G. Thomas and S. P. Vanka: Materials Processing in the Computer Age, Vol. 3, ed. by V. Voller and H. Henein, TMS, Warrendale, PA, (2000), 189.
26) Y. Tanizawa, M. Toyoda, K. Takatani and T. Hamana: *Rev. Metal*., **90** (1993), No. 8, 993.
27) I. Sawada, Y. Kishida, K. Okazawa and H. Tanaka: *Tetsu-to-Hagané*, **79** (1993), No. 2, 16 .
28) I. Sawada, K. Okazawa, E. Takeuchi, K. Shigematsu and H. Tanaka: *Nippon Steel Tech. Rep.*, No. 67, (1995), 7.
29) M. Yao, M. Ichimiya, M. Tamiya, K. Suzuki, K. Sugiyama and R. Mesaki: *Trans. Iron Steel Inst. Jpn.*, **24** (1984), No. 2, s211.
30) M. Yao, M. Ichimiya, S. Kiyohara, K. Suzuki, K. Sugiyama and R. Mesaki: 68th Steelmaking Conf. Proc., AIME, ISS, Warrendale, PA, (1985), 27.
31) B. G. Thomas and F. M. Najjar: *Appl. Math. Model*., **15** (1991), No. 5, 226.
32) D. E. Hershey, B. G. Thomas and F. M. Najjar: *Int. J. Numer. Meth. Fluids,* **17** (1993), No. 1, 23.

33) N. C. Markatos: *Ironmaking Steelmaking*, **16** (1989), No. 4, 266.
34) CFX 4.2: AEA Technology, Pittsburgh, PA, Report, (1998).
35) FLUENT5.1: Fluent Inc., Lebanon, New Hampshire, Report, (2000).
36) T. Hirt: Flow Sciences Inc., Los Alamos, New Mexico, Report, (1999).
37) PHOENICS: CHAM, Wimbledon Village, London, UK, Report, (2000).
38) E. Flender: Magma Gmbh, Aachen, Germany, Report, (2000).
39) M. Cross: Computing & Math Sciences, Maritime Greenwich University, Greenwich, UK, Report, (2000).
40) M. S. Engleman: Fluent Inc., Evanston, IL 60201, Report, (2000).
41) M. Sammonds: UES Software, 175 Admiral Cochrane Dr., Annapolis, MD, Report, (2000).
42) P. Thevoz: CALCOM, EPFL, Lausanne, Switzerland, Report, (2000).
43) M. Yao: Modeling and Control of Casting and Welding Processes, Vol. IV, TMS, Warrendale, PA, (1988), 893.
44) F. M. Najjar, B. G. Thomas and D. E. Hershey: *Metall. Trans. B*, **26B** (1995), No. 4, 749.
45) B. G. Thomas, L. J. Mika and F. M. Najjar: *Metall. Trans. B*, **21B** (1990), No. 2, 387.
46) Y. H. Wang: 10th Process Technology Conf. Proc., Vol. 10, ISS, Warrendale, PA, (1992), 271.
47) L. Wang, H.-G. Lee and P. Hayes: *Steel Res*., **66** (1995), No. 7, 279.
48) H. Bai and B. G. Thomas: 83rd Steelmaking Conf. Proc., Vol. 83, ISS, Warrendale, PA, (2000), 183.
49) B. G. Thomas, A. Denissov and H. Bai: Steelmaking Conf. Proc., Vol. 80, ISS, Warrendale, PA, (1997), 375.
50) H. Bai and B. G. Thomas: *Metall. Mater. Trans. B*, **32B** (2001), No. 2, 253.
51) H. Bai and B. G. Thomas: *Metall. Mater. Trans. B*, **32B** (2001), No. 2, 269.
52) K. Tozaki: Nishiyama Memorial Seminar, ISIJ, Tokyo, (1994).
53) B. G. Thomas, X. Huang and R. C. Sussman: *Metall. Trans. B*, **25B** (1994), No. 4, 527.
54) H. Bai and B. G. Thomas: *Metall. Mater. Trans. B*, (2001), under review.
55) J. Szekely and V. Stanek: *Metall. Trans*., **1** (1970), No. 1, 119.
56) S. Asai and J. Szekely: *Ironmaking Steelmaking*, **3** (1975), No. 3, 205.
57) X. K. Lan, J. M. Khodadadi and F. Shen: *Metall. Mater. Trans. B*, **28B** (1997), No. 2, 321.
58) S. Yokoya, Y. Asako, S. Hara and J. Szekely: *ISIJ Int*., **34** (1994), No. 11, 883.
59) S. Yokoya, R. Westoff, Y. Asako, S. Hara and J. Szekely: *ISIJ Int*., **34** (1994), No. 11, 889.
60) S. Sivaramakrishnan: M. S. Thesis, University of Illinois, (2000).
61) S. Sivaramakrishnan, H. Bai, B. G. Thomas, P. Vanka, P. Dauby and M. Assar: Ironmaking Conf. Proc., Vol. 59, ISS, Warrendale, PA, (2000), 541.
62) R. C. Sussman, M. Burns, X. Huang and B. G. Thomas: 10th Process Technology Conf. Proc., Vol. 10, ISS, Warrendale, PA, (1992), 291.
63) P. Andrzejewski, K.-U. Kohler and W. Pluschkell: *Steel Res*., **63** (1992), No. 6, 242.
64) N. Bessho, R. Yoda, H. Yamasaki, T. Fujii, T. Nozaki and S. Takatori: *Iron Steelmaker* (*ISS Transactions*), **18** (1991), No. 4, 39.
65) N. Bessho, R. Yoda and H. Yamasaki: Proc. 6th Int. Iron Steel Cong., Vol. 3, ISIJ, Tokyo, (1990), 340.
66) B. Grimm, P. Andrzejewski, K. Muller and K.-H. Tacke: *Steel Res*., **70** (1999), No. 10.
67) B. Grimm, P. Andrzejewski, K. Wagner and K.-H. Tacke: *Stahl Eisen*, **115** (1995), (2), 71.
68) R. H. M. G. Nabben, R. P. J. Duursma, A. A. Kamperman and J. L. Lagerberg: *Ironmaking Steelmaking*, **25** (1998), No. 5, 403.
69) M. Yemmou, M. A. A. Azouni and P. Casses: *J. Cryst. Growth*, **128** (1993), No. 4, 1130.
70) J. K. Kim and P. K. RRRohatgi: *Metall. Mater. Trans. B*, **29A** (1998), No. 1, 351.
71) D. M. Stefanescu and A. V. Catalina: *ISIJ Int*., **38** (1998), No. 5, 503.
72) M. R. Aboutalebi, M. Hasan and R. I. L. Guthrie: *Metall. Mater. Trans. B*, **26B** (1995), No. 4, 731.
73) Y. Ho, C. Chen and W. Hwang: *ISIJ Int*., **34** (1994), No. 3, 255.
74) Y. Ho and W. Hwang: *ISIJ Int*., **36** (1996), No. 8, 1030.
75) H. Tanaka, R. Tsujino, A. Imamura, R. Nishihara and J. Konishi: *ISIJ Int*., **34** (1994), No. 6, 498.
76) B. G. Thomas and X. Huang: 76th Steelmaking Conf. Proc., Vol. 76, Warrendale, PA, (1993), 273.
77) Y. Hwang, P. Cha, H. Nam, K. Moon and J. Yoon: *ISIJ Int*., **37** (1997), No. 7, 659.
78) X. Huang and B. G. Thomas: *Can. Metall. Q*., **37** (1998), No. 304, 197.
79) B. Li, T. Okane and T. Umeda: *Metall. Mater. Trans. B*, **31B** (2000), No. 6, 1491.
80) N. Kubo, J. Kubota, M. Suzuki and T. Ishii: *Nippon Steel Tech. Rep*., (1998), No. 164, 1.
81) H. Turkoglu and B. Farouk: *ISIJ Int*., **31** (1991), No. 12, 1371.
82) D. Creech: M. S. Thesis, University of Illinois at Urbana-Champaign, (1998).
83) I. Hamill and T. Lucas: Fluid Flow Phenomena in Metals Processing, Minerals, Metals and Materials Society, Warrendale, PA, (1999), 279.
84) O. J. Ilegbusi and J. Szekely: *ISIJ Int*., **34** (1994), No. 12, 943.
85) H. Bai and B. G. Thomas: *Metall. Mater. Trans. B*, (2001), in press.
86) L. Zhang: *Modelling and Simulation in Materials Science and Engineering*, **8** (2000), No. 4, 463.
87) Y. Sato and K. Sekoguchi: *Int. J. Multiphase Flow*, **2** (1975), No. 1, 79.
88) B. G. Thomas and S. P. Vanka: NSF Design & Manufacturing Grantees Conf., NSF, Washington, D.C., (1999).
89) L. Zhang and S. Taniguchi: *Int. Mater. Rev*., **45** (2000), No. 2, 59.
90) H. Mizukami, S. Hiraki and T. Watanabe: *Tetsu-to-Hagané*, **86** (2000), No. 3, 152.
91) T. Ishii, S. S. Sazhin and M. Makhlouf: *Ironmaking Steelmaking*, **23** (1996), No. 3, 267.
92) K.-H. Spitzer, M. Dubke and K. Schwerdtfeger: *Metall. Mater. Trans. B*, **17B** (1986), No. 2, 119.
93) I. Hoshikawa, T. Saito, M. Kumura, Y. Kaihara, K. Tanikawa, H. Fukumoto and K. Ayata: *Iron Steelmaker* (*ISS Transactions*), **18** (1991), No. 4, 45.
94) N. Genma, T. Soejima, T. Saito, M. Kimura, Y. Kaihara, H. Fukumoto and K. Ayata: *ISIJ Int*., **29** (1989), No. 12, 1056.
95) H. Harada, E. Takeuchi, M. Zeze and H. Tanaka: *Applied Mathematical Modelling*, **22** (1998), No. 11, 873.
96) M. R. Aboutalebi, M. Hasan and R. I. L. Guthrie: *Numer. Heat Transfer, Part A*, **28** (1995), No. 3, 279.
97) C.-A. Gandin, T. Jalanti and M. Rappaz: Modeling of Casting, Welding, and Advanced Solidification Processes, Vol. VIII, ed. by B. G. Thomas and C. Beckermann, TMS, Warrendale, PA, (1998), 363.
98) V. R. Voller, A. D. Brent and C. Prakash: *Int. J. Heat Mass Transfer*, **32** (1989), No. 9, 1719.
99) M. C. Schneider and C. Beckermann: *Metall. Mater. Trans. A*, **26A** (1995), No. 9, 2373.
100) B. G. Thomas, B. Ho and G. Li: Alex McLean Symp. Proc., ISS, Warrendale, PA, (1998), 177.
101) G. D. Lawson, S. C. Sander, W. H. Emling, A. Moitra and B. G. Thomas: Steelmaking Conf. Proc., Vol. 77, ISS, Warrendale, PA, (1994), 329.
102) X. Huang, B. G. Thomas and F. M. Najjar: *Metall. Trans. B*, **23B** (1992), No. 6, 339.
103) B. G. Thomas: Continuous Casting of Steel, Chap.15, ed. by O. Yu, Marcel Dekker, New York, (2000).
104) B. G. Thomas, R. J. O'Malley and D. T. Stone: Modeling of Casting, Welding, and Advanced Solidification Processes, Vol. VIII, ed., by B. G. Thomas and C. Beckermann, TMS, Warrendale, PA, (1998), 1185.
105) J. M. Khodadadi: HTD-Transport Phenoimena in Materials Processing and Manufacturing, Vol. 196, ASME, New York, (1992), 59.
106) J.-E. Lee, T.-J. Yeo, K. H. Oh, J.-K. Yoon and U.-S. Yoon: *Metall. Mater. Trans. A*, **31A** (2000), No. 1, 225 .
107) J. Lee, H. Han, K. OH and J. Yoon: *ISIJ Int*., **39** (1999), No. 5, 435.
108) J. E. Kelly, K. P. Michalek, T. G. O'Connor, B. G. Thomas and J. A.

Dantzig: *Metall. Trans. A*, **19A** (1988), No. 10, 2589.
109) A. Moitra and B. G. Thomas: Steelmaking Proc., Vol. 76, ISS, Warrendale, PA, (1993), 657.
110) I. Ohnaka and Y. Yashima: Modeling of Casting and Welding Processes, Vol. IV, TMS, Warrendale, PA, (1988), 385.
111) B. G. Thomas, A. Moitra and W. R. Storkman: Proc. 6th Int. Iron Steel Cong., Vol. 3, ISIJ, Tokyo, (1990), 348.
112) B. G. Thomas and J. T. Parkman: Thermec 97 Int. Conf. on Thermomechanical Processing of Steel and Other Materials, Vol. 2, ed. by T. Chandra, TMS, Warrendale, PA, (1997), 2279.
113) B. G. Thomas, A. Moitra and R. McDavid: *Iron Steelmaker* (*ISS Transactions*), **23** (1996), No. 4, 57.
114) B. G. Thomas: *ISS Trans*., **16** (1989), No. 12, 53.
115) K. Schwerdtfeger and H. Sha: *Metall. Mater. Trans. B*, **31B** (2000), No. 4, 813.
116) A. Palmaers, A. Etienne and J. Mignon: *Stahl Eisen*, **99** (1979), No. 19, 1039.
117) J. B. Dalin and J. L. Chenot: *Int. J. Num. Meth. Eng*., **25** (1988), No. 1, 147.
118) B. Barber and A. Perkins: *Ironmaking Steelmaking*, **16** (1989), No. 6, 406.
119) K. Okamura and H. Kawashima: Proc. Int. Conf. Comp. Ass. Mat. Design Proc. Simul., ISIJ, Tokyo, (1993), 129.
120) L. Yu: M.S. Thesis, University of Illinois, (2000).
121) M. Uehara, I. V. Samarasekera and J. K. Brimacombe: *Ironmaking Steelmaking*, **13** (1986), No. 3, 138.
122) J. Rottman: *J. Fluid Mech*., **124** (1982), 283.
123) D. Gupta and A. K. Lahiri: *Metall. Trans. B*, **27B** (1996), No. 4, 695.
124) A. Theodorakakos and G. Bergeles: *Metall. Mater. Trans. B*, **29B** (1998), No. 6, 1321.
125) C. W. Hirt and B. D. Nichols: *J. Comput. Phys*., **39** (1981), No. 1, 201.
126) J. Anagnostopoulos and G. Bergeles: *Metall. Mater. Trans. B*, **30B** (1999), No. 6, 1095.
127) C. W. Hirt, A. A. Amsden and J. L. Cook: *Journal of Computational Physics*, **14** (1974), No. 3, 227.
128) K. Takatani, Y. Tanizawa and M. Kawamoto: The 3rd Int. Symp. on Electromag. Processing of Materials 2000, ISIJ, Tokyo, (2000), 91.
129) G. A. Panaras, A. Theodorakakos and G. Bergeles: *Metall. Mater. Trans. B*, **29B** (1998), No. 5, 1117.
130) R. McDavid and B. G. Thomas: *Metall. Trans. B*, **27B** (1996), No. 4, 672.
131) R. McDavid: Masters Thesis, University of Illinois at Urbana-Champaign, (1994).
132) D. Bouris and G. Bergeles: *Metall. Mater. Trans. B*, **29B** (1998), No. 3, 641.
133) X. Huang and B. G. Thomas: *Metall. Trans*., **24B** (1993), No. 2, 379.
134) X. Huang and B. G. Thomas: *Metall. Trans. B*, **27B** (1996), No. 4, 617.
135) B. G. Thomas: *Iron Steelmaker*, **24** (1997), No. 12, 83.
136) H. Yang, L. Zhao, X. Zhang, K. Deng, W. Li and Y. Gan: *Metall. Mater. Trans. B*, **29B** (1998), No. 6, 1345.
137) I. Steinbach and G. J. Schmitz: Modeling of Casting, Welding, and Advanced Solidification Processes, Vol. VIII, ed., by B. G. Thomas and C. Beckermann, TMS, Warrendale, PA, (1998), 521.
138) K. Miyazawa and K. Schwerdtfeger: *Arch. Eisenhüttenwes.*, **52** (1981), No. 11, 415.
139) H. Eisermann and K. Schwerdtfeger: Proc. Julian Szekely Mem. Symp. Mater. Process, ed. by H. Y. Sohn, J. W. Evans and D. Apelian, TMS, Warrendale, PA, (1997), 383.
140) G. Lesoult and S. Sella: *Solid State Phenomena*, **3** (1988), 167.
141) T. Kajitani, J.-M. Drezet and M. Rappaz: *Metall. Mater. Trans*., (2001), in press.
142) M. C. Flemings: *ISIJ Inter*., **40** (2000), No. 9, 833.
143) C. Beckermann: Fleming Symp., TMS, Warrendale, PA, (2000).